Hindawi Publishing Corporation
Advances in Optical Technologies
Volume 2008, Article ID 251718, 8 pages
doi:10.1155/2008/251718

Research Article

Ultrashort Laser Pulse Heating of Nanoparticles: Comparison of Theoretical Approaches

Renat R. Letfullin,[1] Thomas F. George,[2] Galen C. Duree,[1] and Brett M. Bollinger[1]

[1] *Department of Physics and Optical Engineering, Rose-Hulman Institute of Technology, 5500 Wabash Avenue, Terre Haute, IN 47803, USA*
[2] *Office of the Chancellor and Center for Nanoscience, Department of Chemistry and Biochemistry and Department of Physics and Astronomy, University of Missouri—St. Louis, One University Boulevard, St. Louis, MO 63121, USA*

Correspondence should be addressed to Renat R. Letfullin, letfullin@rose-hulman.edu

Received 28 January 2008; Accepted 11 March 2008

Recommended by Stoyan Tanev

The interaction between nanoparticles and ultrashort laser pulses holds great interest in laser nanomedicine, introducing such possibilities as selective cell targeting to create highly localized cell damage. Two models are studied to describe the laser pulse interaction with nanoparticles in the femtosecond, picosecond, and nanosecond regimes. The first is a two-temperature model using two coupled diffusion equations: one describing the heat conduction of electrons, and the other that of the lattice. The second model is a one-temperature model utilizing a heat diffusion equation for the phonon subsystem and applying a uniform heating approximation throughout the particle volume. A comparison of the two modeling strategies shows that the two-temperature model gives a good approximation for the femtosecond mode, but fails to accurately describe the laser heating for longer pulses. On the contrary, the simpler one-temperature model provides an adequate description of the laser heating of nanoparticles in the femtosecond, picosecond, and nanosecond modes.

1. INTRODUCTION

The application of ultrashort laser pulse thermal-based killing of abnormal cells (e.g., cancer cells) targeted with absorbing nanoparticles (e.g., solid gold nanospheres, nanoshells, or nanorods) is becoming an extensive area of research [1–3]. High laser energies in ultrashort pulses can be concentrated on an extremely small biological mass infused with metallic nanoparticles, and the heat gained by the particles used as a protein denaturizing agent in targeted cells. Photons emitted from the ultrashort laser pulse are absorbed by free electrons within the metal via inverse Bremsstrahlung and transferred to the lattice subsystem, and then to the surrounding medium. Injected into biological media, nanoparticles provide a highly selective method for ablating target cells when coupled with appropriate laser pulse duration.

Traditional knowledge of laser-nanoparticle interactions has necessitated specialized models for each case, dependent upon the laser pulse duration. Previous research has recognized the existence of these conditions and dual-temperature models for the ultrashort laser pulse mode calculating electron, and lattice subsystem temperatures are readily available (see, e.g., [4, 5]). Pulses of longer duration are modeled using a uniform heating model [6–9], an appropriate approximation for pulse durations greatly exceeding the electron-phonon coupling time. On a dimensional scale, this approximation is reasonable for particles sizes not much larger than a laser wavelength, which is completely applicable for the heating of nanoparticles.

Ultrashort pulses, specifically those in the femtosecond and picosecond ranges, impose several challenges in modeling material response. Free electrons with minimal capacity for heat are the first to absorb energy, rapidly attaining high temperatures, and transferring thermal energy to the material lattice. These processes do not occur instantaneously: time must be allowed for the cooling of the electrons and the heating of the lattice. In our work, electron cooling and lattice heating have time delays on the order of femtoseconds and picoseconds, respectively. Ultrashort laser pulses end before the transfer of energy to the lattice is complete, requiring two-temperature models in order to describe the

further conversion of energy from electron excitation to heat within the lattice system.

In the present paper, we demonstrate that a simpler, one-temperature model (OTM) utilizing the uniform heating approximation is appropriate for understanding ultrashort laser pulse interactions with metal nanoparticles. The approximation may be used in this situation due to the extremely small size of nanoparticles in comparison to the wavelength of laser radiation. Using this idea, the time delay between the electron and lattice interactions will be bypassed, and the simpler model will ultimately yield results similar to the two-temperature model (TTM). Comparative simulations of the two modeling approaches are performed in this paper to confirm OTM as an appropriate approximation for nanoparticle heating in the femtosecond, picosecond, and nanosecond regimes, thus providing an effective modeling method for further nanomedicine research to explore.

2. THEORETICAL BACKGROUND

2.1. One-temperature model

During the interaction of a laser pulse of intensity I_0 and pulse duration τ_L with a metal nanoparticle of radius r_0, the laser energy is absorbed by free electrons due to the inverse Bremsstrahlung, and then transferred from the electron gas into the lattice. In OTM, it is assumed that the electron heat transfer into phonon subsystem is very fast, that is, the electron and lattice temperatures are equal $T_e = T_s$ at any moment of the time. In this approximation, we can limit our description to only one lattice temperature distribution, $T_s(t,r)$, which could be found by numerical solution of a heat-mass transfer equation between the particle and the surrounding medium:

$$\frac{dT_s(t,r)}{dt} = \frac{\mu_s(T_s)}{\rho_s C_s(T_s)}\Delta T_s(t,r) + \frac{Q(t,r)}{\rho_s C_s(T_s)} - j_D(T_s)S_0 + \frac{3L}{r_0 C_s(T_s)}\frac{dr_0}{dt}, \quad (1)$$

where $\Delta = \partial^2/\partial x^2 + \partial^2/\partial y^2 + \partial^2/\partial z^2$ is a Laplace operator; $\mu_s(T_s)$, $C(T_s)$, L, ρ_s, and r_0 are, respectively, the heat conductivity, specific heat, evaporation heat, density, and radius of the nanoparticle; $Q(t,r)$ is a heat source; $j_D(T_s)$ is the heat lost from the surface of the nanoparticle into the surrounding medium; $S_0 = 4\pi r_0^2$ is the particle surface area.

The power density of energy generation in the particle $Q(t,r)$ due to radiation energy absorption is generally nonuniform throughout the particle volume, with the nonuniformity being dependent on the size and optical constants of the particle. Since for nanoparticles $2\pi r_0/\lambda < 1$, we can assume that $Q(t,r)$ is uniform throughout the particle volume [6–9], and it can be described by the equation

$$Q(t,r_0) = \frac{3K_{\text{abs}}(r_0,\lambda)I_0 f(t)}{4r_0}, \quad (2)$$

where $K_{\text{abs}}(r_0,\lambda)$ is the absorption efficiency of the nanoparticle as a function of laser wavelength λ and particle radius r_0, and $f(t)$ is a time profile of a laser pulse.

Heat exchange between the nanoparticle surface and the surrounding medium is rapid, and heat loss becomes substantial for relatively long laser pulses. Assuming that the heat lost from the surface of nanoparticle occurs only due to heat diffusion into surrounding medium, the energy flux density $j_D(T_s)$ removed from the particle surface can be expressed as a nonlinear function of temperature [7–9]:

$$j_D(T_s) = \frac{\mu_\infty T_s}{(s+1)r_0^2 C_s(T_s)\rho_s}\left[\left(\frac{T_s}{T_\infty}\right)^{s+1} - 1\right], \quad (3)$$

where μ_∞ is the heat conductivity of the surrounding medium at normal temperature T_∞, and the power exponent $s = \text{const}$ depends on the thermal properties of the surrounding medium.

After integration over the volume for the spherically symmetric case and transition to a uniform temperature over the particle volume, the equation which describes the kinetics of laser heating of the nanoparticle and results from (1) takes the following form [7–9]:

$$\frac{dT_s}{dt} = \frac{3K_{\text{abs}}I_0 f(t)}{4r_0 C_s(T_s)\rho_s} - \frac{\mu_\infty T_s}{(s+1)r_0^2 C_s(T_s)\rho_s}\left[\left(\frac{T_s}{T_\infty}\right)^{s+1} - 1\right] + \frac{3L}{r_0 C_s(T_s)}\frac{dr_0}{dt}. \quad (4)$$

Here, the first term on the right side of the equation describes the heat generation into the spherical volume due to laser energy absorption by the nanoparticle. The second term describes the energy losses from the surface of the particle into the surrounding medium due to the heat diffusion process. The last term describes the energy losses due to the evaporation of the particle. This evaporation depends on the laser pulse characteristics and particle properties, and it can be realized in five different regimes (see, e.g., [8, 9]): free-molecular, convective, diffusive, gas-dynamic, and explosive [3] modes of evaporation. For example, within the approximation of free-molecular flow, the evaporation term in (4) can be written as

$$4\pi r_0^2 \frac{dr_0}{dt}\rho_s = -\eta 4\pi r_0^2 V_s(T_s)\rho_v(T_s), \quad (5)$$

where η is the accommodation coefficient, and $V_s(T_s)$ and $\rho_s(T_s)$ are, respectively, the average velocity and density of the vapor at temperature T_s. If the heating of the nanoparticle occurs below the temperature of phase transition in the particle material, the third term on the right side of (4) can be neglected.

2.2. Two-temperature model

In TTM, the temperature relaxation in time and sample depth can be modeled by two-coupled diffusion equations: one describing the heat conduction of electrons and the

other that in the lattice. Both equations are connected by a term that is proportional to the electron-phonon coupling constant γ and to the temperature difference between electrons and lattice, originally proposed by Anisimov et al. [10]. We modify this original set of equations, adding a heat exchange term between the surface of the particle and the surrounding medium. Also, we are taking into account the dependence of the thermophysical parameters of electrons, particle, and surrounding medium on temperature during the laser treatment, as presented in Table 1. The modified set of equations describing the heating of electron and lattice subsystems and the energy transfer between particle and surrounding medium has the form

$$C_e(T_e)\frac{\partial T_e}{\partial t} = -\frac{\partial Q(z)}{\partial z} - \gamma(T_e - T_s) + S,$$
$$C_i(T_s)\frac{\partial T_s}{\partial t} = \gamma(T_e - T_s) - \frac{\mu_\infty T_s}{(s+1)r_0^2 C_s(T_s)\rho_s}\left[\left(\frac{T_s}{T_\infty}\right)^{s+1} - 1\right], \quad (6)$$

where $Q(z) = -k_e(\partial T_e/\partial z)$ is the heat flux; z is the direction perpendicular to the target surface; k_e is the electron thermal conductivity; $S = I_0 f(t)\alpha\exp(-\alpha z)$ is the laser heating source term; α is the material absorption coefficient; $C_e(T_e)$ and $C_i(T_s)$ are the temperature-dependent heat capacities (per unit volume) of the electron and lattice subsystems. The expressions for the temperature dependence of the heat capacities, as well as the values for the electron-phonon coupling constant γ and material data, are listed in Table 1.

3. RESULTS AND DISCUSSION

Comparative simulations using the models described above have been performed for the laser heating of a gold nanoparticle with radius $r_0 = 20$ nm in a surrounding medium of water. The same set of input data presented in Table 1 was used for the calculations in both models. The temperature dependences of the electron heat capacity for the gold, specific heat, and thermal conductivity for the water were obtained by interpolating the experimental data available in the literature (references are listed in Table 1). As can be seen from the table, the electron heat capacity is much less than the lattice heat capacity, and therefore electrons can be heated to very high transient temperatures. Then, the evolution of the electron temperature involves energy transfer to the lattice and energy losses due to the electron heat transport into the target. The electron-phonon coupling process has several characteristic time scales: electron thermalization time τ_e, electron cooling time τ_c, lattice heating time τ_i, and duration of the laser pulse τ_L. The relationship between them defines three different regimes of the laser-metal interaction—femtosecond, picosecond, and nanosecond modes of heating.

3.1. Femtosecond pulses

TTM and OTM have been solved numerically to predict the time dependence of the electron and lattice temperatures in the femtosecond mode when the laser pulse duration is shorter than the electron thermalization and cooling times, $\tau_L \ll \tau_e, \tau_c$. The calculations were performed for a laser pulse energy density of $E = 1.0$ mJ/cm^2 and pulse duration of $\tau_L = 60$ femtoseconds. The time profile of the femtosecond laser pulse given in Table 1 and shown in Figure 1(b) (solid curve) corresponds to the experimentally observed output from an amplified Ti: sapphire laser (Legend-HE from Coherent Inc., Santa Clara, Calif, USA). The laser flux is chosen at the level 1.0 mJ/cm^2 to provide the cell lethality during a single laser pulse. The results of the simulations for the heating of a gold nanoparticle by a femtosecond laser pulse are shown in Figures 1 and 2. Figure 1(b) displays the results obtained by TTM, and Figure 1(b) presents the results of OTM simulations. A comparison of these two models is shown in Figure 2.

As follows from Figure 1(a), thermal equilibrium among the excited electrons with equilibrium temperature $T_e \approx 3300$ K for a given laser fluence is established within 175 femtoseconds. We should note that the equilibrium temperature for electrons is reached long after the end of a laser pulse, which had a duration of 60 femtoseconds. The electrons remain in the thermal equilibrium state from several hundred femtoseconds up to 1 picosecond (see Figure 3(a)). Then, the electrons cool exclusively by coupling to the lattice, resulting in a linear decay of the electron temperature during the first 10 picoseconds (Figure 3(a)). Our simulations agreed with the electron relaxation time measured in [15] for femtosecond pulse excitation of a DNA-modified gold nanoparticle.

The slow rate of electron heat diffusion into the phonon subsystem on the femtosecond time scale results in a delay of about 100 femtoseconds in the heating of the bulk sample (dashed curve in Figure 1(a)). Once the electron thermal equilibrium is established, a hot electron bath raises the temperature of the cold lattice up to 1090 K for a given laser energy density $E = 1$ mJ/cm^2.

The results of heating the gold nanoparticle obtained by OTM are demonstrated in Figure 1(b). This figure also shows the femtosecond laser pulse time profile used in the calculations. Comparative simulations for the evolution of the nanoparticle temperature using both models under the same conditions are presented in Figure 2. It follows from these simulations that both models demonstrate the same scenario in the heating kinetics of a metal nanoparticle by a femtosecond laser pulse. Both models reveal approximately a 100-femtosecond time delay in the heating of the particle, followed by a maximum lattice temperature of around 1090 K within 175 femtoseconds after the end of a laser pulse. Even the maximum values of the particle temperature predicted by both models are the same (see Figure 2). The saturation parts in the lattice temperature curves are explained by negligibly small heat diffusion from the surface of the nanoparticle into the surrounding medium on the femtosecond time scale. A slight difference in the slopes of the temperature curves within the first 100 femtoeconds of heating occurs due to the assumption made in OTM that the electron heat transfer into the lattice subsystem is very fast. Because of this, the particle temperature in OTM promptly

Table 1: Input parameters used for simulations in both models.

Parameters	Magnitude and units	Reference
Laser pulse shape	$f(t) = \exp[-(at-b)^2 - (at-c)^2]$, a, b, c = const	
Energy density	$E = 10^{-3}\ \mathrm{J/cm^2}$	
Volume density of the gold	$\rho_0 = 0.0193\ \mathrm{kg/cm^3}$	[11]
Electron heat capacity (gold)	$C_e(T_e) = aT_e^4 - bT_e^3 + cT_e^2 - dT_e + e$, $\left(\frac{\mathrm{J}}{\mathrm{K^2 cm^3}}\right)$ $a = 6.0 \times 10^{-17}$, $b = 3.0 \times 10^{-12}$, $c = 5.07 \times 10^{-8}$, $d = 6.7589 \times 10^{-5}$, $e = 7.207 \times 10^{-2}$,	[12]
Electron-phonon coupling constant for gold	$\gamma = 2.27 \times 10^{10}\ \frac{\mathrm{W}}{\mathrm{K\,cm^3}}$	[13]
Gold specific heat	$C = 129\ \frac{\mathrm{J}}{\mathrm{K\,kg}}$	
Specific heat of water	$C_w(T_s) = a(1 + b(T_s - 293\ \mathrm{K}))$, $\left(\frac{\mathrm{J}}{\mathrm{K\,kg}}\right)$ $a = 4182.0$, $b = 1.016 \times 10^{-4}$.	
Radius of gold nanoparticle	$r_0 = 20\ \mathrm{nm}$	
Absorption efficiency of gold nanoparticle	$K_{\mathrm{abs}} = 4.0195$ ($r_0 = 20$ and $\lambda = 528\ \mathrm{nm}$)	[2, 14]
Absorption coefficient of gold nanoparticle	$\alpha = 8.736 \times 10^5\ \mathrm{cm^{-1}}$ ($r_0 = 20\ \mathrm{nm}$ and $\lambda = 528\ \mathrm{nm}$)	[14]
Power exponent	$s = 1.0$	
Thermal conductivity of water	$\mu_0(T_s) = a(1 + b(T_s - T_\infty))$, $\left(\frac{\mathrm{W}}{\mathrm{K\,cm}}\right)$ $a = 0.00597$, $b = 1.78 \times 10^{-3}$.	

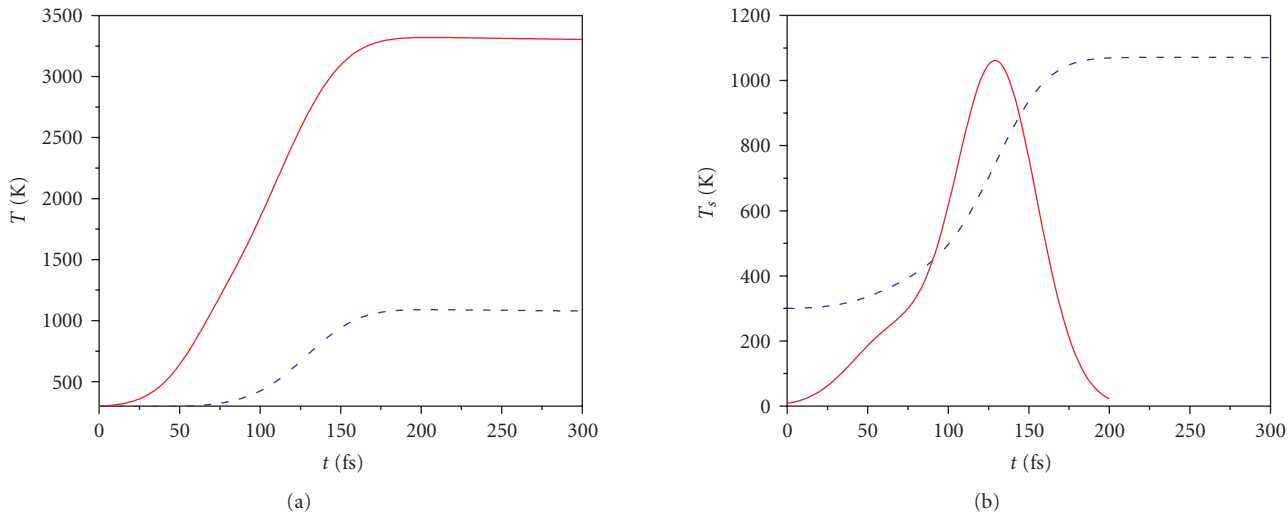

Figure 1: (a) Electron (solid curve) and lattice (dashed curve) temperature evolutions on the femtosecond time scale for a gold nanoparticle predicted by TTM. (b) Evolution of the nanoparticle temperature (dashed curve) after the femtosecond laser pulse, predicted by OTM, and laser pulse shape (solid curve).

follows electron thermal behavior. A comparison of these two models shows that the simpler OTM gives the same results as the more precise TTM. Thus, OTM provides an adequate description of the laser heating of nanoparticles in the femtosecond regime.

3.2. *Picosecond pulses*

In this mode, the constants a, b, and c in the time profile for the laser pulse have been chosen to provide the laser pulse width of 60 picoseconds at FWHM with the same pulse shape

Table 2: Thermophysical characteristics of the gold particle and surrounding biological tissue.

Material	Specific heat C (J/K kg)	Interval of T (K)	Thermal conductivity μ_0 (W/m K)	Thermal diffusivity χ (m^2/s)
Gold	129	273–373	318	1.18×10^{-4}
Water	$4181.6-4215.6$ $C(T) = 4182(1 + 1.016 \times 10^{-4}(T - 293\,\text{K}))$	273–373	$0.597-0.682$ $\mu(T) = 0.597(1 + 1.78 \times 10^{-3}(T - T_\infty))$	1.43×10^{-7}
Human prostate	3740	310	0.529	
Blood	3645–3897	273–373	0.48–0.6	1.6×10^{-7}
Fat	2975	273–373	0.185–0.233	
Tumor	3160	310	0.561	
Skin		273–373	0.210–0.410	

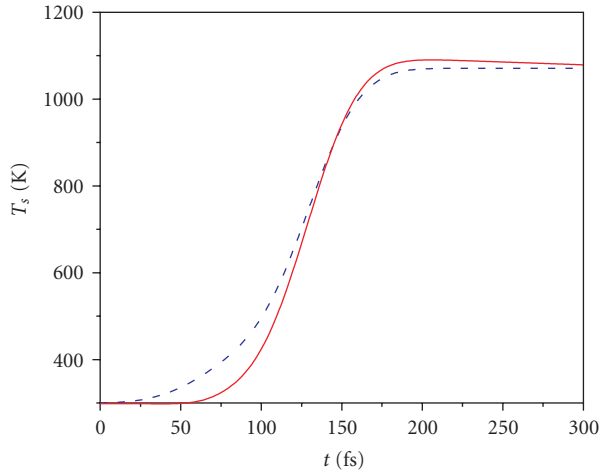

Figure 2: Comparison of nanoparticle temperature evolutions after the 60 femtoseconds laser pulse-predicted TTM (solid curve) and one-temperature model (dashed curve).

listed in Table 1 and shown in Figure 1(b). As can be seen from Figures 1(b) and 3(b), in the picosecond regime the electron thermalization time τ_e and electron cooling time τ_c are much less than the duration τ_L of the 60 picoesonds laser pulse. Hence, during the first 10 picoseconds, the electron subsystem has already been completely cooled (Figure 3(a)), and the electron temperature above the ambient no longer exists for the considered picosecond mode of heating. This is confirmed by our calculations presented on Figure 3(b) (dashed curve). Thus, TTM provides a very good approximation for the femtosecomd mode as soon as the electron temperature exists, but it fails to describe the laser heating of nanoparticles for longer pulse durations in the picosecond and nanosecond regimes.

Opposite to TTM, OTM describes the picosecond heating kinetics very well. A typical time evolution of the particle temperature predicted by OTM on the picosecond time scale is displayed in Figure 3(b) (solid curve) for the same material constants listed in Table 1. The main feature is the appearance of heat lost from the surface of the nanoparticle into the surrounding medium on the picosecond time scale. After about 200 picoseconds, cooling of the nanoparticle begins due to heat diffusion into the water. The maximum temperature reached by a 20-nm gold particle for the given laser pulse is 995 K. This temperature is sufficient to initiate any thermal killing mechanisms in cancer cells.

3.3. Nanosecond pulses

For laser heating of metal nanoparticles in the nanosecond regime, the characteristic lattice heating time τ_i is much smaller than the laser pulse duration: $\tau_L \gg \tau_i$. This means that, the temperature inside the nanoparticle is nearly uniform over the whole particle at the time scale of the laser pulse duration τ_L. In this case, the electron and lattice temperatures are equal, $T_e = T_s$, so that the homogeneous heating of the particle and quasisteady heat exchange with the surrounding medium can be described by just OTM. The characteristic lattice heating time τ_i required for the formation of a quasistationary temperature profile across the nanoparticle can be estimated from the formula $\tau_i = r_0^2/4\chi$, where r_0 is the particle radius and χ the thermal diffusivity of the particle material. For gold nanoparticle ($\chi = 1.18 \times 10^{-4}$ m^2/s) with radii $r_0 = 20$–30 nm, the lattice heat diffusion time is $\tau_i \sim 2 \times 10^{-12}$ s $\ll \tau_L \sim 10^{-8}$ s.

Sample calculations have been carried out using OTM for gold nanoparticles with radii $r_0 = 30$–35 nm in different surrounding biomedia for an incident laser pulse of energy $E = 10$ mJ/cm^2 and pulse duration $\tau_L = 8$ nanoseconds with the time profile shown in Figure 1(b). The laser pulse profile and duration 8 nanoseconds have been chosen to be close to those used in previous experiments [2]. The laser flux chosen is ten times higher than in the regimes considered above to provide approximately the same maximum nanoparticle temperature as observed for femtosecond and picosecond laser heating. We should note that 10 mJ/cm^2 is comparable to the laser fluence currently used in the photothermolysis of cancer cells [1, 3]. The kinetics of heating and cooling the gold nanoparticle are demonstrated in Figure 4, where (a) illustrates the time dynamics of laser heating of a 30-nm gold particle in different biological media: blood, human prostate, tumor, and fat. The thermophysical characteristics of gold and biological surrounding media for different temperatures are listed in Table 2. Figure 4(b) shows results of thermal calculations for a 35-nm gold particle, which is heated and cooled in water at different heat transfer rates s.

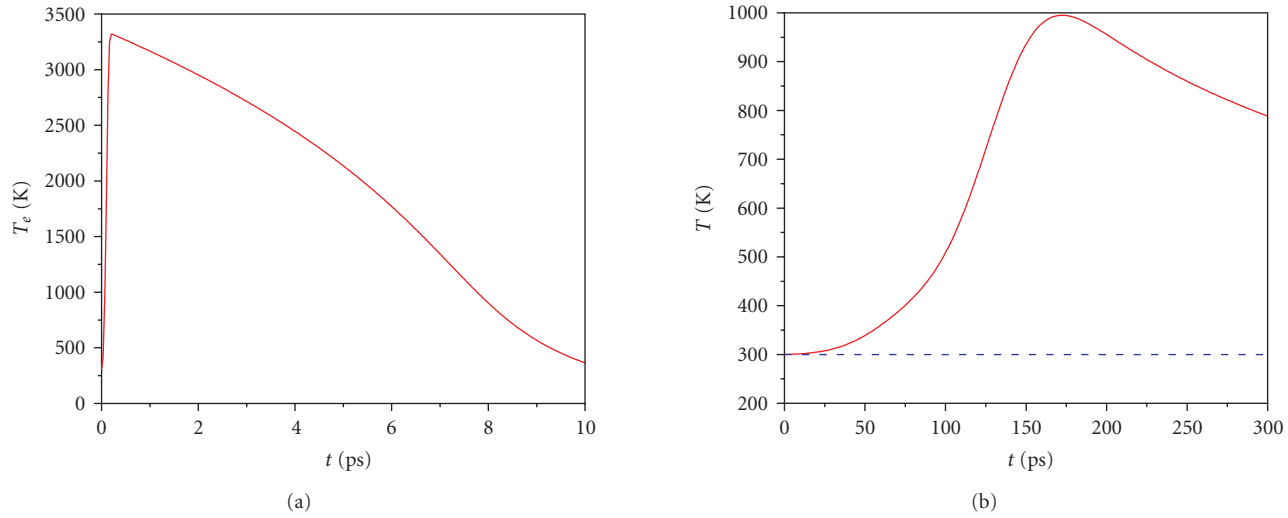

Figure 3: (a) Electron temperature relaxation on the picosecond time scale. (b) Temperature time distributions for a gold nanoparticle predicted by OTM (solid curve) and TTM (dashed curve) after the 60 picoseconds laser pulse.

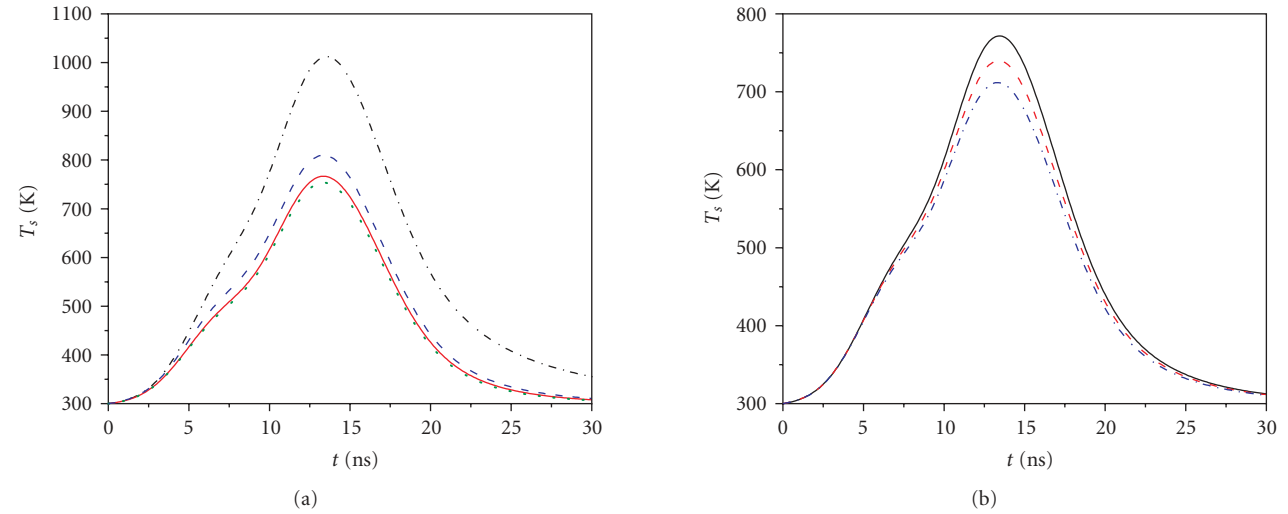

Figure 4: Kinetics of heating and cooling of a gold nanoparticle by a nanosecond laser pulse of energy density 10 mJ/cm^2 and duration 8 nanoseconds. Calculations have been made by using OTM. (a) Illustration of the time dynamics of laser heating of a 30-nm gold particle in different biological media: fat (dashed-dotted curve), blood (dashed curve), tumor (solid curve), and prostate (dotted curve). (b) Results of thermal calculations for a 35-nm gold particle: heating and cooling in the water surrounding medium at different heat transfer rates $s : s = 1.0$ (solid curve), $s = 1.25$ (dashed curve), and $s = 1.5$ (dashed-dotted curve).

It follows from these calculations that during the laser pulse duration the transfer of heat from the nanoparticle into the surrounding media is slight, and the particle rapidly reaches a high temperature. The heating rate is about 10^{12} Ks^{-1}. The temperature of the particle continues to rise even after the end of the laser pulse. The highest temperature, 770 K, for a given laser pulse fluence is observed for the heating time of 13.5 nanoseconds, when the laser pulse has already degraded (see Figure 4(a)). After that time, the transfer of heat from the particle to the surrounding medium becomes increasingly important, since the energy source is no longer present in the system. The temperature of the particle and surrounding medium remains high ($\sim$ 400 K) up to 20 nanoseconds, exceeding the laser pulse duration by 2.5 times. The total time for one cycle (heating from the initial temperature 300 K to maximum temperature, followed by cooling back to the initial temperature) is about 30 nanoseconds.

We have also examined the effect of different biological surroundings on the laser heating dynamics of 30 nm gold particles. Four biomedia were used: namely, blood, human prostate, tumor, and fat. Results of computer simulations of the time-temperature profiles of gold nanoparticles in various biological media, performed by using OTM, are plotted in Figure 4(a). As follow from our calculations, the laser heating and temperature behavior of the gold

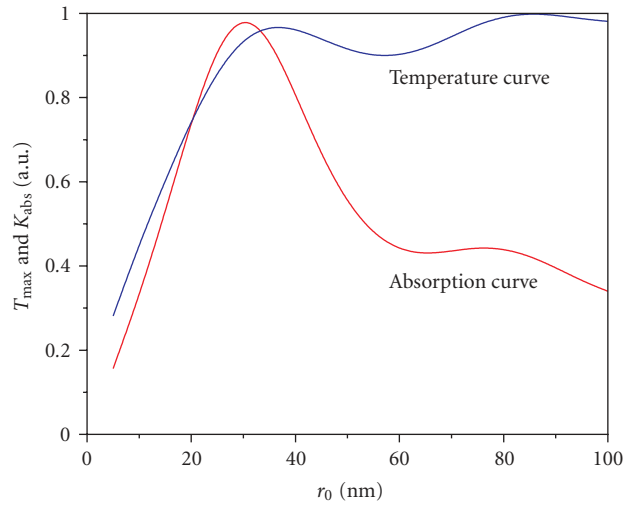

FIGURE 5: Nondimensional (a.u.) absorption efficiency K_{abs} and maximal temperature T_{max} curves as a function of the particle's radius for the gold nanoparticles in blood heated by a laser pulse of energy density 10 mJ/cm^2 and duration 8 nanoseconds.

nanoparticles in blood, prostate, and tumor are comparable to the water surrounding medium case, since the thermodynamic properties of those media are very close to each other (see Table 2). This means that for the thermal calculations of laser heating of biological media, the thermal properties of water can be used if the water content in the media is high. But the heating of a gold nanoparticle in fat is substantially different from the water case, since the fat has low-thermal characteristics. Here, we observe higher overheating of the particle at the same energy level and duration of the laser pulse due to the relatively low-thermal conductivity of fat as compared to other biomedia.

The temperature dynamics of the particle is sensitive to the power exponent s used in the temperature dependence of the heat lost from the surface of the nanoparticle into the surrounding medium, that is, $(j_D(T_s)$ in (3) (see Figure 4(b)). The value of $s = 1$ better corresponds to the real biological surrounding. The power $s > 1$ describes the medium with high thermophysical characteristics, like the cooling liquids and metals. The medium with $s < 1$ has a low thermal conductivity and can be used as a thermal isolator.

It is interesting to investigate the effect of the particle's radius on the temperature dynamics of the nanoparticle heated by the nanosecond laser radiation in the biological surroundings. There are two competitive factors here. On one hand, according to the Mie diffraction theory, the absorption efficiency of the gold nanoparticle drops with the decreasing size of the particle. On the other hand, the heating rate increases for smaller particles as follows from (4). To find which factor has a stronger effect on the effective laser heating of a gold nanoparticle, we have calculated the maximal temperature profile for different nanoparticle radii in blood and compared it to the gold nanoparticle absorption curve. The results of these simulations are performed by using OTM and presented in Figure 5. It follows from this figure that the optical effect is much stronger than the thermal effect when the radius of nanoparticle is less than 35 nm. In the radii range 1–35 nm, the overheating effect of the particle behaves according to the absorption efficiency. For a radius of 35 nm, the thermal processes dominate over the optical properties. For large radii ($\geq$ 35 nm), the maximal temperature profile is saturated with oscillations, repeating the maxima and minima of the absorption curve. The saturation of the maximal temperature curve for large particle radii is explained by the balance between heating of the particle due to absorption of laser energy and energy losses from the surface of the particle due to heat diffusion into the surrounding biological medium.

4. CONCLUSIONS AND SUMMARY

The comparative analysis of OTM and TTM for heating of a metal nanoparticle in the femtosecond, picosecond, and nanosecond regimes has shown that

(i) in the femtosecond mode, the thermal equilibrium among the excited electrons is established within the first 175 femtoesonds, long after the end of the laser pulse duration;
(ii) the electrons remain in the thermal equilibrium state up to 1 picosecond;
(iii) both models demonstrate the same scenario in the heating kinetics of a metal nanoparticle by a femtosecond laser pulse: about a 100-femtosecond time delay in the heating of the particle is observed, until reaching a maximum lattice temperature and saturation in temperature curves after 175 femtoeconds;
(iv) the electron cooling time due to coupling to the lattice is about 10 picoecond, which imposes an upper time limit for TTM application;
(v) TTM gives a very good approximation for the femtosecomd mode while an electron temperature exists, but it fails to describe the laser heating of nanoparticles for longer pulse durations in the picosecond and nanosecond regimes;
(vi) OTM shows that the heat lost from the surface of the nanoparticle into the surrounding medium becomes noticeable after 200 picoseconds;
(vii) the heating of a metal nanoparticle by a nanosecond laser pulse in fat provides higher particle overheating than in blood, prostate, and water as surrounding media due to the thermally isolating property of the fat;
(viii) the optical properties of the nanoparticle have a much stronger effect on the heating dynamics in the nanosecond mode than the thermal effects when the radius of the particle is less than 35 nm. For larger particles, the thermal processes dominate the optical properties, and the temperature curve is determined by the balance between heating of the nanoparticle and energy losses from the surface of the particle due to heat diffusion into the surrounding biological medium.

Thus, the comparison of the two models shows that OTM provides an adequate description of the laser heating of

nanoparticles in the femtosecond, picosecond, and nanosecond regimes.

ACKNOWLEDGMENT

This work has been supported by the Lilly Foundation Grant AA0000010.

REFERENCES

[1] C. M. Pitsillides, E. K. Joe, X. Wei, R. R. Anderson, and C. P. Lin, "Selective cell targeting with light-absorbing microparticles and nanoparticles," *Biophysical Journal*, vol. 84, no. 6, pp. 4023–4032, 2003.

[2] V. P. Zharov, R. R. Letfullin, and E. N. Galitovskaya, "Microbubbles-overlapping mode for laser killing of cancer cells with absorbing nanoparticle clusters," *Journal of Physics D*, vol. 38, no. 15, pp. 2571–2581, 2005.

[3] R. R. Letfullin, C. Joenathan, T. F. George, and V. P. Zharov, "Cancer cell killing by laser-induced thermal explosion of nanoparticles," *Journal of Nanomedicine*, vol. 1, pp. 473–480, 2006.

[4] J. L. Wu, C. M. Wang, and G. M. Zhang, "Ultrafast optical response of the Au-BaO thin film stimulated by femtosecond pulse laser," *Journal of Applied Physics*, vol. 83, no. 12, pp. 7855–7859, 1998.

[5] B. N. Chichkov, C. Momma, S. Nolte, F. von Alvensleben, and A. Tünnermann, "Femtosecond, picosecond and nanosecond laser ablation of solids," *Applied Physics A*, vol. 63, no. 2, pp. 109–115, 1996.

[6] V. K. Pustovalov, "Theoretical study of heating of spherical nanoparticle in media by short laser pulses," *Chemical Physics*, vol. 308, no. 1-2, pp. 103–108, 2005.

[7] R. R. Letfullin and V. I. Igoshin, "Multipass optical reactor for laser processing of disperse materials," *Quantum Electronics*, vol. 25, no. 7, pp. 684–689, 1995.

[8] R. R. Letfullin, "Solid aerosols into the strong laser fields," *Bulletin of the Samara State Technical University. Physical-Mathematical Sciences*, no. 4, pp. 243–263, 1996.

[9] R. R. Letfullin and V. I. Igoshin, "Theoretical modeling of plasma formation and generation of electromagnetic fields in the gas-dispersed media under the action of laser radiation," *Trudy FIAN*, vol. 217, pp. 112–135, 1993.

[10] S. I. Anisimov, B. L. Kapeliovich, and T. L. Perel'man, "Electron emission from metal surfaces exposed to ultrashort laser pulses," *Soviet Physics JETP*, vol. 39, pp. 375–377, 1974.

[11] R. B. Ross, *Metallic Materials Specification Handbook*, Chapman & Hall, London, UK, 4th edition, 1992.

[12] Z. Lin, L. V. Zhigilei, and V. Celli, "Electron-phonon coupling and electron heat capacity of metals under conditions of strong electron-phonon nonequilibrium," *Physical Review B*, vol. 77, no. 7, Article ID 075133, 17 pages, 2008.

[13] J. Hohlfeld, S.-S. Wellershoff, J. Güdde, U. Conrad, V. Jähnke, and E. Matthias, "Electron and lattice dynamics following optical excitation of metals," *Chemical Physics*, vol. 251, no. 1–3, pp. 237–258, 2000.

[14] P. K. Jain, K. S. Lee, I. H. El-Sayed, and M. A. El-Sayed, "Calculated absorption and scattering properties of gold nanoparticles of different size, shape, and composition: applications in biological imaging and biomedicine," *Journal of Physical Chemistry B*, vol. 110, no. 14, pp. 7238–7248, 2006.

[15] P. K. Jain, W. Qian, and M. A. El-Sayed, "Ultrafast cooling of photoexcited electrons in gold nanoparticle-thiolated DNA conjugates involves the dissociation of the gold-thiol bond," *Journal of the American Chemical Society*, vol. 128, no. 7, pp. 2426–2433, 2006.